NANOSYSTEMS: PHYSICS, CHEMISTRY, MATHEMATICS, 2018, 9 (4), P. 521–531

Capillary filling of carbon nanotubes by $BiCl_3$: TEM and MD insight

E. A. Anumol[1], F. L. Deepak[1], A. N. Enyashin[2]

[1]Nanostructured Materials Group, Department of Advanced Electron Microscopy, Imaging and Spectroscopy, International Iberian Nanotechnology Laboratory (INL), Braga, Portugal

[2]Institute of Solid State Chemistry UB RAS, Ekaterinburg, Russia

leonard.francis@inl.int; enyashin@ihim.uran.ru

PACS 34.30.+h, 34.35.+a, 05.70.Np **DOI 10.17586/2220-8054-2018-9-4-521-531**

Among numerous trichlorides, the melt of $BiCl_3$ is a distinctly molecular liquid with a relatively low melting point, yet, with a high surface tension. Therefore, the attractiveness of a simple capillary filling technique for fabrication of nanosized $BiCl_3$ by dispersion within a nanocapillary needs a special investigation. Here, we report the successful synthesis and the transmission electron microscopy characterization of the hybrids consisting of multi-walled carbon nanotubes and endohedral $BiCl_3$ crystallites. The main peculiarities of imbibition into carbon nanotubes and an intricate internal organization of molten $BiCl_3$ are established using the developed 4-site force-field model of $BiCl_3$ and consequent molecular dynamics simulations at nanosecond time scale.

Keywords: Bismuth trichloride, carbon nanotubes, capillary, TEM characterization, MD simulations.

Received: 18 July 2018

1. Introduction

The main attribute of Carbon nanotubes – the cavity – suggests their capillary activity, assigning their role as proper templates for the growth of other one-dimensional nanostructures in its interior or serve as containers for nanocargos. Open-ended carbon nanotubes, soon after their discovery, were theoretically characterized as "molecular straws" capable of capturing molecules from a vapor or a fluid due to the interactions akin to those in wetting and capillary action [1]. This prediction was successfully proved by the first experiment on filling of multi-walled carbon nanotubes with molten lead in air [2].

Nowadays, the capillary filling technique is routinely employed for encapsulation of fusible metals and compounds into carbon nanotubes, forming endohedral hybrids subsequent to annealing at temperatures above the melting points and followed by cooling. Considerable progress has been attained in both the production and the TEM characterization of ultra-thin halide, oxide and sulfide nanowires encapsulated in single- and multi-walled nanotubes [3–6].

The wetting of the nanotubular interior by the melt of a quasi-two-dimensional inorganic compound can yield the single-walled inorganic nanotubes, too. Hence, the properties of conventional inorganic compounds confined within carbon nanotubes can be modified not only at the level of simple size scaling, but as well at the level of structural organization. Currently, it is the only way to obtain the nanotubes of halides (PbI_2 [7], ZnI_2, CeI_3, $CeCl_3$, $TbCl_3$ [8], GdI_3 [9], BiI_3 [10]) in large and stable amounts, since the walls of carbon hosts are excellent protectors from environmental moisture.

Being active intermediators or accumulators of charge carriers, the walls of metallic carbon nanotubes can act as nanoreactors, forcing the encapsulated compounds to undergo a further polymorphic or chemical transformation. Particularly, the crystal lattices of many halides, when confined in the one-dimensional space, tend to adopt an unusual ionic coordination [11], whereas LaI_3 transforms formally into a different stoichiometric composition LaI_2 [12], which may lead to the rise of materials with new electronic, luminescent and magnetic properties. The capillary filling of carbon nanotubes by $HgCl_2$ [13], NiI_2 [14] and GdI_3 [15] is accompanied by the metal reduction, which, in the case of iodides, manifests itself as the final product containing also the carbon nanotubes filled either by iodine or by metal nanowires.

Endohedral hybrids of inorganic compounds and carbon nanotubes fabricated using capillary filling technique are promising advanced materials for biomedical applications. As the locked vehicles the carbon nanotubes are capable of improving the long-term stability of encapsulated materials *in vivo*. They can convey within organisms such nanocargos like radionuclides serving as radiolabels [16] or anticancer agents [17]. Potentially, carbon nanotubes dispersing at their interior a heavy metal compound could become the components of radioprotective composites.

Bismuth trichloride $BiCl_3$ is a compound with a relatively low melting point ($T_m = 507$ K) among other metal trichlorides [18]. Presumably, the application of this compound as an eco-friendly catalyst in organic

synthesis [19,20] and as a core-building component in antimicrobial complex agents [21] could be expanded at the nanoscale level, e.g. by nanodispersion using encapsulation into carbon nanotubes.

Here, we explore the abilities of capillary filling technique for fabrication of endohedral hybrids $BiCl_3$@MWCNT – encapsulates of crystalline $BiCl_3$ in multi-walled carbon nanotubes (MWCNTs). Notwithstanding the low T_m, molten $BiCl_3$ has the challengingly high values of surface tension ($\sigma = 65$ mJ/m^2 at $T = 1.1T_m$) and viscosity ($\eta = 26$ mPa·s at $T = 1.1T_m$) [22], which could suppress the capillary activity of carbon nanotubes. Compared to the other molten trichlorides, the compound also demonstrates anomalously high values of electrical conductivity [18] and has a tendency for disproportionation at elevated temperatures [23], not yet clarified in the presence of an extended carbon surface. However, despite all these challenges, our joint results from both the transmission electron microscopy (TEM)/scanning transmission electron microscopy (STEM) characterization and the molecular dynamics (MD) simulations confirm a successful capillary action of MWCNTs regarding the molten $BiCl_3$, yielding stoichiometric rod-like or tubular-like $BiCl_3$ nanostructures shielded by the carbon shell.

2. Experimental part

2.1. Procedure of capillary filling

Bismuth(III) chloride, anhydrous, 99.999 % (metals basis) was purchased from Alfa Aesar and used without further purification. MWCNTs were purchased from Nanocyl SA, Belgium and US Research Nanomaterial, Inc, USA. The as-purchased nanotubes were open ended. The encapsulation of $BiCl_3$ into MWCNTs was carried out by capillary filling. Bismuth trichloride along with MWCNTs, both sealed under vacuum in a quartz ampule, were annealed in a furnace above the melting point of $BiCl_3$ and subsequently cooled to room temperature. The detailed conditions for the synthesis of $BiCl_3$@MWCNT hybrids are given in Table 1 and Fig. 1. The final synthetic products were not treated and were characterized as they have been obtained.

TABLE 1. Synthesis conditions for $BiCl_3$@MWCNT hybrids. The histograms for diameter distributions of parent MWCNTs are visualized in Fig. 1

Sample	CNT:$BiCl_3$ (mg)	Temperature (°C)	Heating Rate (°C/min)	Duration (h)
$BiCl_3$ MWCNT 1	13:300	350	2	72
$BiCl_3$ MWCNT 2	10:300	350	2	72
$BiCl_3$ MWCNT 2A	15:300	500	2	168
$BiCl_3$ MWCNT 3	11:300	350	2	72
$BiCl_3$ MWCNT 4	10:300	350	2	72

2.2. Microscopy characterization

Samples for TEM/STEM analysis were prepared on porous carbon film 300 mesh Cu grids. An FEI Titan Themis 60 – 300 kV electron microscope, operated at 80 kV, equipped with probe and image correctors and a monochromator, was used for TEM and STEM imaging. EDX spectra were obtained using a Super-X detector and acquired and analyzed using Bruker Esprit software. Crystal models were constructed using Crystal maker software and diffraction patterns were simulated using Single crystal software.

2.3. Computational details

Capillary filling of carbon nanotubes was simulated using MD and was considered as an imbibition of a finite drop-like amount of melt. The starting model for drop of molten $BiCl_3$ was designed as a fragment of crystalline $BiCl_3$ consisting of 250 or 500 stoichiometric units and annealed in series at MD temperatures $T = 300$ K, 533 K, 623 K as well as 693 K and 773 K. The drop $(BiCl_3)_{500}$ was employed for validation of the force-field as described below. The final structure of the drop $(BiCl_3)_{250}$ equilibrated at $T = 623$ K was used further as the starting model to study the imbibition at the same temperature. MWCNT model was designed as a rigid cluster of double-walled (20,20)@(25,25) carbon nanotube (DWCNT) composed of 75 unit cells (internal and external radii of 13.56 and 16.95 Å, 13500 atoms in total). The edge surface of the $BiCl_3$ drop was installed initially at 3 Å from the apex of DWCNT.

MD simulations have been performed using in-house code as for canonical ensembles (NVT). In all simulations the temperature was controlled with the velocity scaling. Newton's equations of motion were integrated with the MD time step of 2.5 fs via the Verlet leapfrog algorithm during 500,000 steps for the annealing and during 1,380,000 steps for the imbibition.

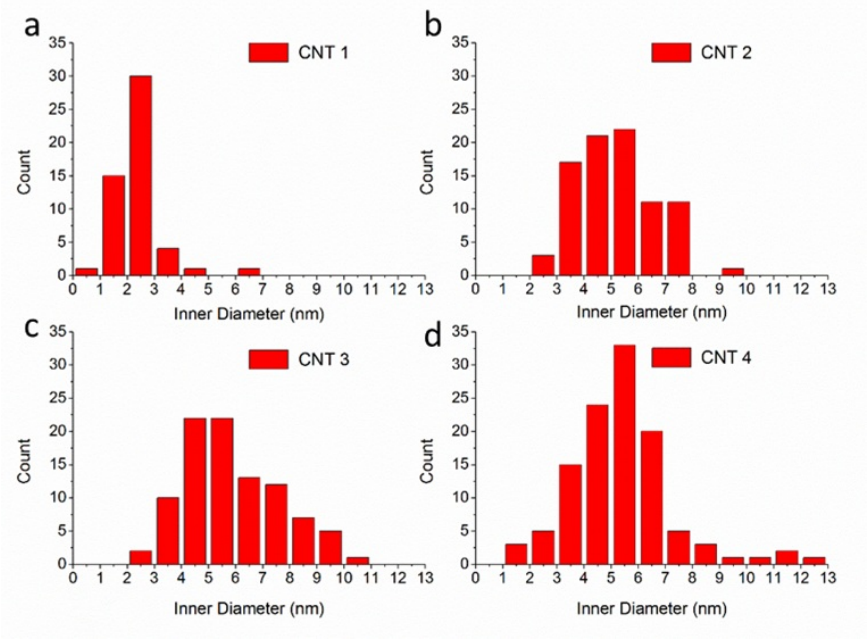

FIG. 1. Diameter distributions for multi-walled carbon nanotubes (MWCNT) in the samples employed for the synthesis of $BiCl_3$@MWCNT composites (see Table 1)

The force-field level of theory was applied for these nanosecond MD simulations. The model of liquid $BiCl_3$ was represented as an ensemble of the rigid 4-site molecules with the geometry matching that within $BiCl_3$ crystal ($r_{Bi-Cl} = 2.464$ Å, $\varphi_{Cl-Bi-Cl} = 94.46°$ [24]). Therefore, intramolecular interactions were not considered, while intermolecular $BiCl_3$ interactions were described using Coulomb and Lennard-Jones potentials as parametrized in framework of Universal Force Field (UFF) [25]. Atomic charges on Bi and Cl were taken to be equal +2.1 e and +0.7 e, which allow a tolerant reproduction of the sublimation enthalpy [26] and the specific electrical conductivity of molten $BiCl_3$ (*vide infra*) [[27]. Interatomic interactions between $BiCl_3$ melt and DWCNT were described using Lennard-Jones potentials in UFF parametrization. The truncation at 25 Å for all short-range non-bonded interactions was used, while the long-range electrostatic interactions were computed without any restriction and approximation.

Visualization of atomic structure and MD trajectories was performed using VMD software [28].

3. Results and discussion

3.1. Morphology and composition of $BiCl_3$@MWCNT

Since a direct visualization of the melt imbibition by the nanotubes is not possible using current TEM characterization, we have focused on characterization of the final products. Extending the study to other molten halides, $BiCl_3$ was encapsulated within the MWCNTs by annealing of a mixture of $BiCl_3$ and MWCNT at typical temperature of 350 °C in vacuum sealed quartz ampules. Encapsulation was observed in all the samples of MWCNTs used. Fig. 2 shows the low magnification image of the composite $BiCl_3$@MWCNT with tube-like and rod-like $BiCl_3$ nanostructures encapsulated within the cavities of MWCNTs.

Figure 3 shows the elemental map distribution of Bi and Cl within the cavity of an individual MWCNT along with the corresponding EDX spectrum, which on quantification gives Bi:Cl ratio consistent with that of $BiCl_3$. The filling was predominantly amorphous in nature along with some crystalline $BiCl_3$. The analysis of HRTEM image of the crystalline filling indicates the presence of orthorhombic $BiCl_3$ crystal (ICSD PDF Number: 00-024-1003) within MWCNT (Fig. 4). Both the tube- and rod-like morphologies of $BiCl_3$ were observed in the case of $BiCl_3$ encapsulation within MWCNTs.

Hence, all experiments with the capillary filling of MWCNTs by molten $BiCl_3$ have been successful irrespective of the peculiarities of the synthesis, especially, related to the diameter distribution of MWCNTs. All set of characterization techniques ensured that, the stoichiometric composition of the encapsulated $BiCl_3$ is preserved at the experimentally employed elevated temperatures.

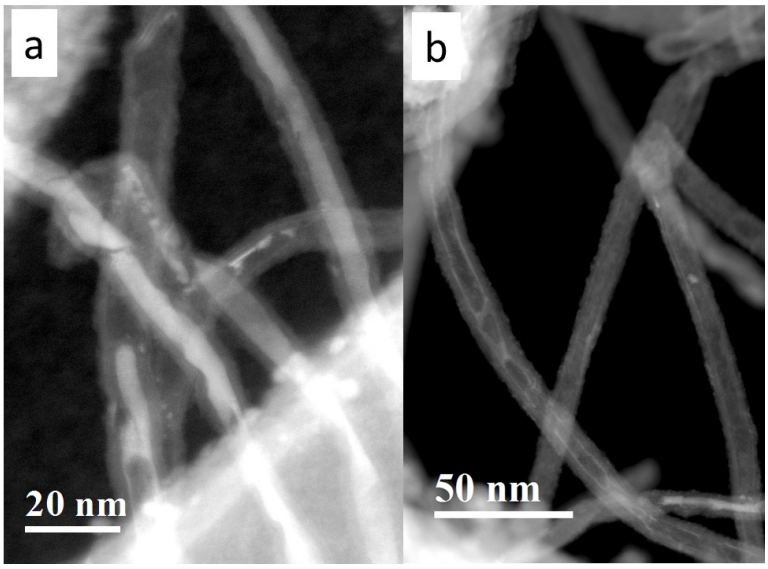

FIG. 2. The HAADF-STEM characterization of the composite $BiCl_3$@MWCNT, unveiling both a rod-like(a) and a tube-like (b) encapsulation of $BiCl_3$ into MWCNTs

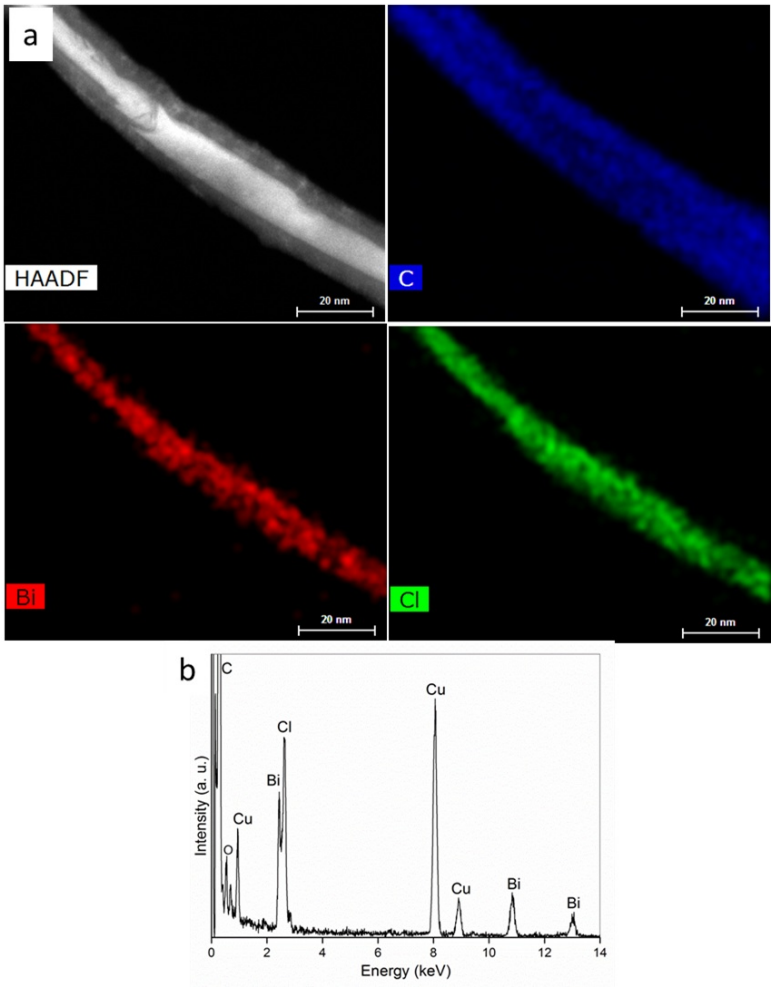

FIG. 3. Individual $BiCl_3$@MWCNT hybrid with a rod-like encapsulation of $BiCl_3$: a) HAADF-STEM image and EDX mappings of C, Bi and Cl elements; b) EDX spectrum corresponding to the panel (a)

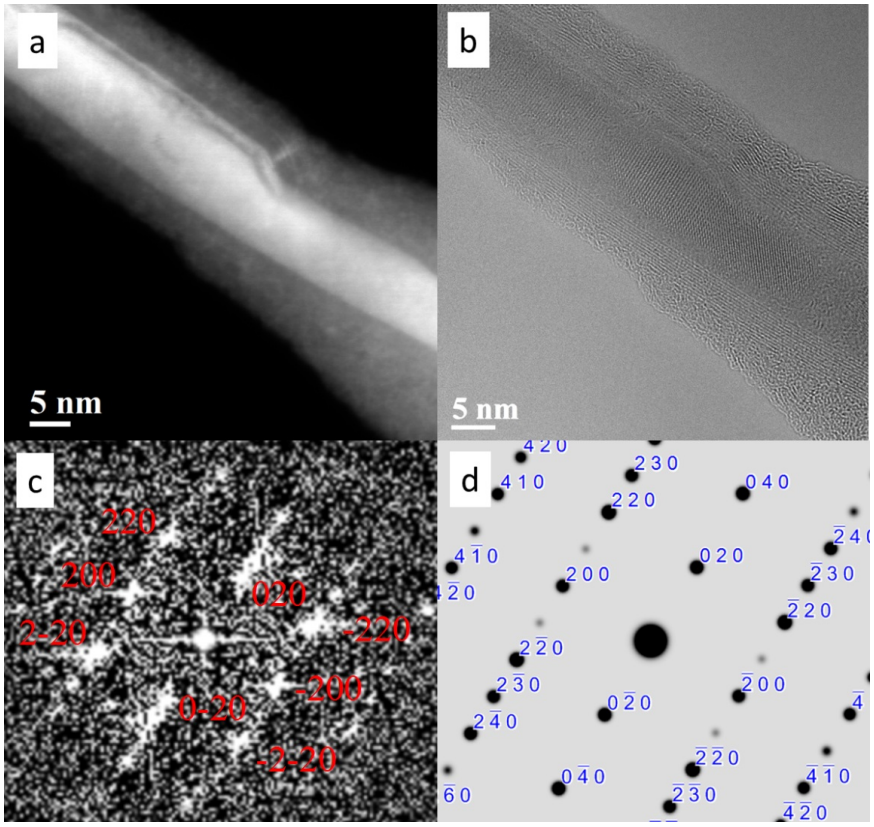

FIG. 4. Structural analysis of a $BiCl_3$ nanorod encapsulated within the MWCNT: a) HAADF-STEM image and b) AC-TEM image of a $BiCl_3$ crystal inside MWCNT; c) is the corresponding FFT which shows that the crystal orientation is [001]; d) the simulated diffraction pattern of the [001] zone axis of orthorhombic $BiCl_3$, which matches with the FFT pattern in the panel (c)

3.2. Validation of force-field for liquid $BiCl_3$

Notwithstanding a high surface tension of molten $BiCl_3$, our TEM characterization testifies clearly that, the capillary activity of MWCNTs is sufficient enough to employ the capillary filling technique for fabrication of $BiCl_3$@MWCNT hybrids. Yet, the filling process by such a tensed liquid might have some peculiarities at the nanoscopic level, which cannot be established experimentally. To gain insights into the mechanism of this process at the atomistic level, the force-field model was evaluated and approved for liquid $BiCl_3$.

Both X-ray and neutron diffractions on the solid crystal unveil an anisotropy in Bi-Cl bond lengths, suggesting an aggregation of molecular-like $BiCl_3$ units [24], where a Bi atom is strongly bonded to three Cl atoms and less strongly to five more. Neutron diffraction on the melt of $BiCl_3$ [18] and electron diffraction on the vapor of $BiCl_3$ [29] indicate a Bi ion coordination of $\sim$3, confirming that the $BiCl_3$ molecules are the building blocks for the solid $BiCl_3$. Though, as a molecular liquid among trichlorides, this compound demonstrates anomalously high values of electrical conductivity and surface tension [18].

To strengthen the credibility of our empirical force-field and to testify the dominantly molecular organization of molten $BiCl_3$ (Fig. 5a,b), such quantitative proofs as the self-diffusion coefficients D for Bi and Cl atoms and the corresponding molar conductivity Λ_m have been received by analysis of obtained MD trajectories using Nernst–Einstein's equation:

$$\Lambda_m = \frac{F^2}{R_G T}\left(v_+ D_+ z_+^2 + v_- D_- z_-^2\right), \quad D = \lim_{t\to\infty} \frac{\langle\langle |\vec{r}_i(t) - \vec{r}_i(0)|^2 \rangle\rangle}{6t},$$

where F is the Faraday constant, R_G is the gas constant, $v+$ and $v-$ are the number of cations and anions per formula unit of electrolyte, $z+$ and $z-$ are the ion charges, t is the MD time and r is the radius vector of an ion.

The data on D(Bi), D(Cl) and Λ_m collected at different temperatures T are listed in Table 2. They are found to be in fair agreement with available experimental data and, to some extent, exceeding the accuracy of another theoretical *ab initio* based MD study, which has considered the evolution of the $Bi_{16}Cl_{48}$ supercell during 220

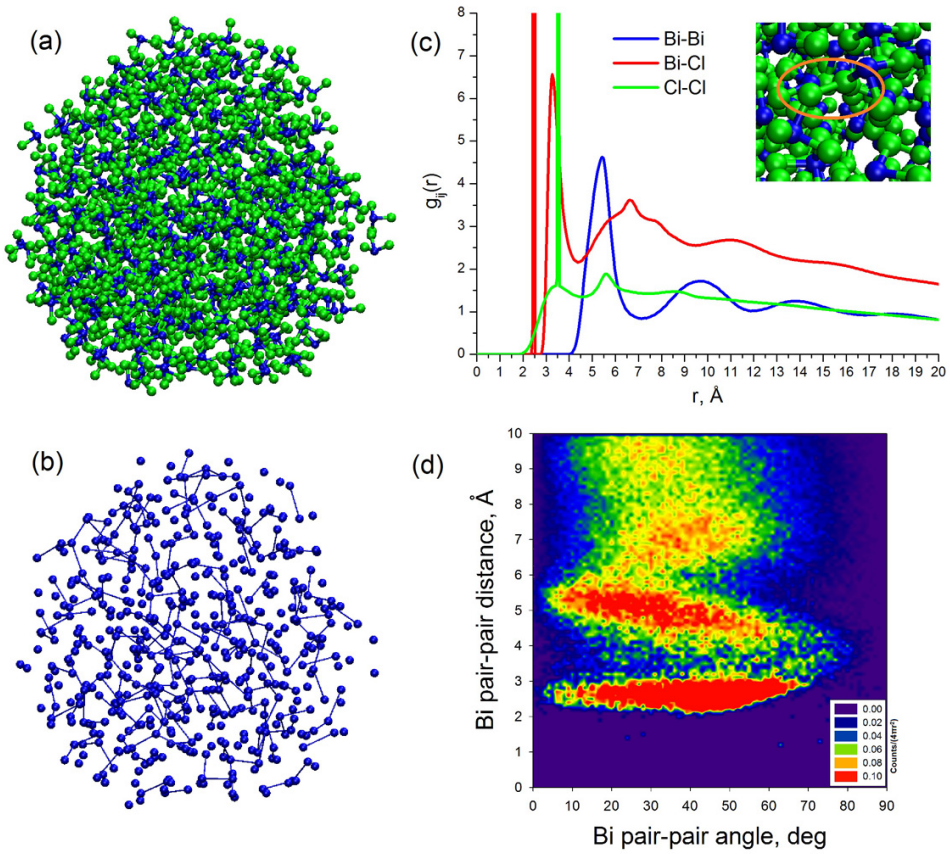

FIG. 5. Structural properties of molten $BiCl_3$ obtained using MD annealing of a $(BiCl_3)_{500}$ drop at $T = 623$ K: (a) ball-and-stick rendering with Bi and Cl atoms painted in blue and green; (b) visualization of only Bi atoms within the drop; (c) radial distribution functions $g_{ij}(r)$ for all types of atomic pairs within the drop, an ultra-short Cl–Cl pair is rendered in inset; (d) angle-resolved radial distribution function of the nearest-neighbor Bi-Bi pairs within the drop

ps [27]. Indeed, our approach might be more successful, since the much larger statistics can be collected for estimation of self-diffusion coefficients using the force-field based MD simulations. On the other hand, our model implies a tight relation between mobility of Bi and Cl atoms, since the rigidity of $BiCl_3$ unit is assumed. Hence, D(Bi) and D(Cl) observed here at the same temperature share a close value, which is in contrast to the data from *ab initio* MD simulations suggesting a larger mobility of Cl atoms, comparing to that of Bi atoms [27].

TABLE 2. Self-diffusion coefficients D and molar conductivity Λ_m for molten $BiCl_3$ at different temperatures obtained from our force-field MD simulations, from experimental data and from *ab initio* MD simulations after [27]

T, K	our work			Exp. [27]	theor. [27]		
	D(Bi)10^{10} (m^2/s)	D(Cl)10^{10} (m^2/s)	Λ_m ($\Omega^{-1}cm^{-1}$)	Λ_m ($\Omega^{-1}cm^{-1}$)	D(Bi)10^{10} (m^2/s)	D(Cl)10^{10} (m^2/s)	Λ_m ($\Omega^{-1}cm^{-1}$)
533	3.3	3.7	0.42	0.433	4.9	8.5	0.9
623	7.0	7.1	0.74	0.551	8.2	15.0	1.2
693	12.4	12.4	1.18	0.585	15.0	25.9	1.5
773	13.8	14.4	1.19	0.556	24.7	44.2	2.0

One should realize that, despite of all advantages, our model of the rigid $BiCl_3$ molecules is valuable and may be employed for MD simulations at relatively low temperatures up to ~700 K, since at elevated temperatures above ~733 K the thermal dissociation of $BiCl_3$ takes place, releasing possibly BiCl species in vapor and polynuclear

complex ions in liquid state [30]. Henceforth, our discussion is limited for $T = 623$ K – a typical temperature used for the capillary filling of MWCNTs.

3.3. Structural organization of molten $BiCl_3$

Expectedly, the radial distribution functions $g_{ij}(r)$ plotted using MD trajectories demonstrate two artifacts – the narrow peaks at the distances $r = 2.46$ Å and 3.62 Å corresponding to the rigid intramolecular Bi-Cl and Cl–Cl distances, respectively (Fig. 5c). Otherwise, the $g_{ij}(r)$ profiles are characterized by several smoothed maxima. The latter are very pronounced for Bi–Bi and Bi–Cl pairs up to the distances of ∼18 Å, providing evidence for a possible ordered organization at intermediate range in the Bi part of the amorphous melt via the Bi–Cl–Bi bridging. Indeed, direct visualization of the Bi part with interatomic Bi–Bi distances up to 5.5 Å (first maximum of $g_{BiBi}(r)$) unveils a confused network (Fig. 5b), consisting of dimer-, triplet-like clusters, zigzag or branched chains. The clustering degree within the melt can be viewed quantitatively, analyzing mutual orientation between all two nearest Bi–Bi neighbors – the pairs – using the map of their angle-resolved radial distribution function (Fig. 5d). In the absence of any positional correlation between the couple of such Bi–Bi pairs at short distances or in the case of total disorder the distribution function is equal to zero. However, the map for molten $BiCl_3$ demonstrates the distinct preferences in orientation of the Bi–Bi pairs, extending even beyond 7 Å. A wide angular distribution ∼15 – 65° in orientation of the Bi–Bi pairs agrees with the previously visualized stochastic chain-like organization of the Bi part.

Thus, our study uncovers unexpectedly a structural organization of the $BiCl_3$ molecules at intermediate range order. This phenomenon relates the molecular melt of $BiCl_3$ to the melts of clearly expressed ionic nature. Noteworthy, the map of angle-resolved radial distribution function for Bi–Bi pairs in $BiCl_3$ is reminiscent of the relative maps for Pb^{2+}–Pb^{2+} cationic pairs in molten PbI_2, assembling the V-shaped triplets, and Gd^{3+}–Gd^{3+} cationic pairs in molten $GdCl_3$, assembling an amorphous 3D network [31]. Therefore, the internal structure of $BiCl_3$ may impose a significant kinetic obstacle for capillary activity of a nanotube like it was observed during imbibition of molten PbI_2 by carbon and BN nanotubes [32] or molten $GdCl_3$ by WS_2 nanotubes [33].

Meanwhile, the $g_{ij}(r)$ profile for Cl–Cl pair demonstrates another interesting peculiarity as a shoulder from ∼2 Å to 3.62 Å (Fig. 5c and inset). This means that a part of Cl atoms can be found closer to each to other than the intramolecular Cl–Cl distance in $BiCl_3$ molecule, and almost approaching the bond length 2.00 Å in molecular chlorine. Therefore, our simple force-field model points to a structural predisposition of molten $BiCl_3$ for partial dissociation with gassing of Cl_2 at higher temperatures [30].

3.4. Imbibition of molten $BiCl_3$ by MWCNT

MD simulations of imbibition of molten $BiCl_3$ by DWCNT confirm a slow dynamics of capillary filling, obstructed by two factors: poor wettability of carbon surface and internal organization of the melt (Fig. 6). The melt penetration proceeds very slowly during the first MD period until ∼2500 ps. At the initial stage of imbibition, the convex meniscus is formed, which is preserved during all MD simulation. Molecules of $BiCl_3$ exclusively enter the cavity and none are adsorbed at the external surface of nanotube. During this period, only a half of the drop is imbibed (Fig. 7a). In contrast, the second MD period is very rapid, and the other half of the drop is imbibed during ∼300 ps. It starts, when the diameter of outer segment of the drop becomes comparable to the diameter of the absorbed part, i.e. becomes slightly smaller, than the inner diameter of nanotube. At this stage the exponential acceleration of imbibition can be observed, which is not essentially constrained by the friction due to the high smoothness of the graphene-like surface. Such slippage causes a rapid cruise of the drop. Obviously, it would continue far away from the entrance point along the channel of a semi-infinite nanotube. Yet, in our model the drop slows down, reaching the opposite open end of nanotube, and then returns to the entrance point. Here, its cruise is oscillating in a dampened manner. Noteworthy, the once entered drop does not leave the cavity of nanotube anymore.

Analyzing the kinetics of imbibition, the invalidity of the Lucas and Washburn theory for a capillary flow is registered (Fig. 7a). The classical theory establishes the dependence of penetrated atoms $\langle N \rangle$ on the time of capillary action t as $\langle N \rangle \sim \sqrt{t}$ for the case of a non-compressible Newtonian liquid, while for molten $BiCl_3$ the relation between $\langle N \rangle$ and t is nearly linear. Such dependence is observed for the liquids with a specific internal structure [31], which coincides with our discussion on the structure of molten $BiCl_3$.

The penetration kinetics can be also traced numerically using the axial (along nanotube) velocity of the drop (Fig. 7b). The variation in axial velocity of the drop's barycenter during the MD simulation amply illustrates two basic stages distinguished above: more or less slack invasion of the melt at a near-zero in average velocity and, finally, exponential growth of velocity to ∼70 m/s.

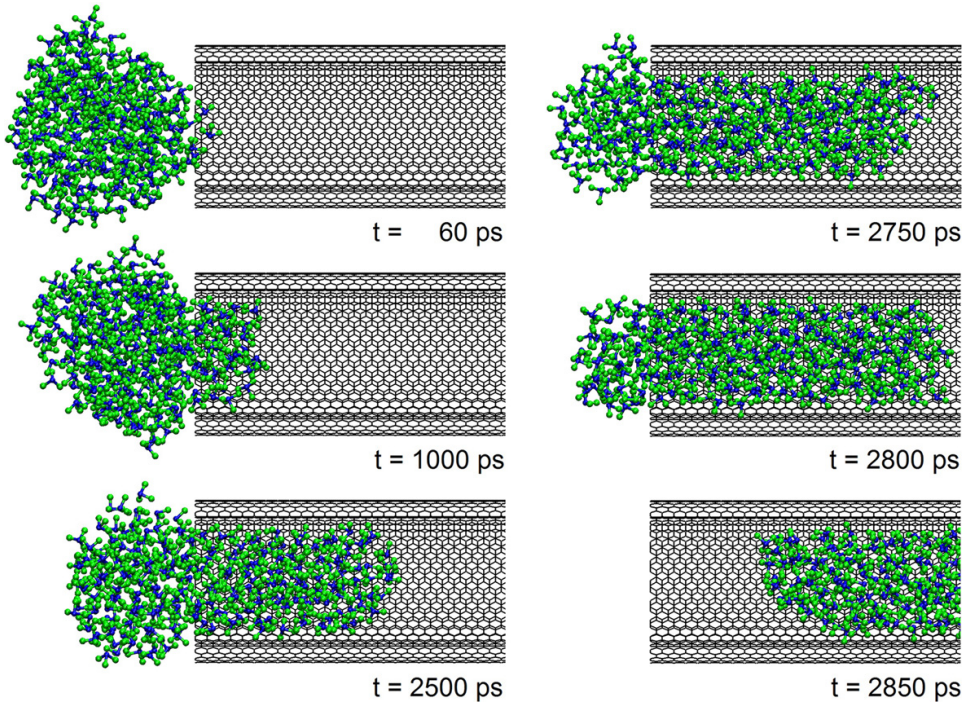

FIG. 6. Snapshots of MD simulation at $T = 623$ K for imbibition of the $(BiCl_3)_{250}$ drop into a (20,20)@(25,25) DWCNT. Bi and Cl atoms are painted in blue and green, while the network of C–C bonds is in black. Frontal part of the nanotube wall is removed for clearness. Full MD movie is accessible via link `https://youtu.be/CLMNa9gBMmg` or on request to the authors

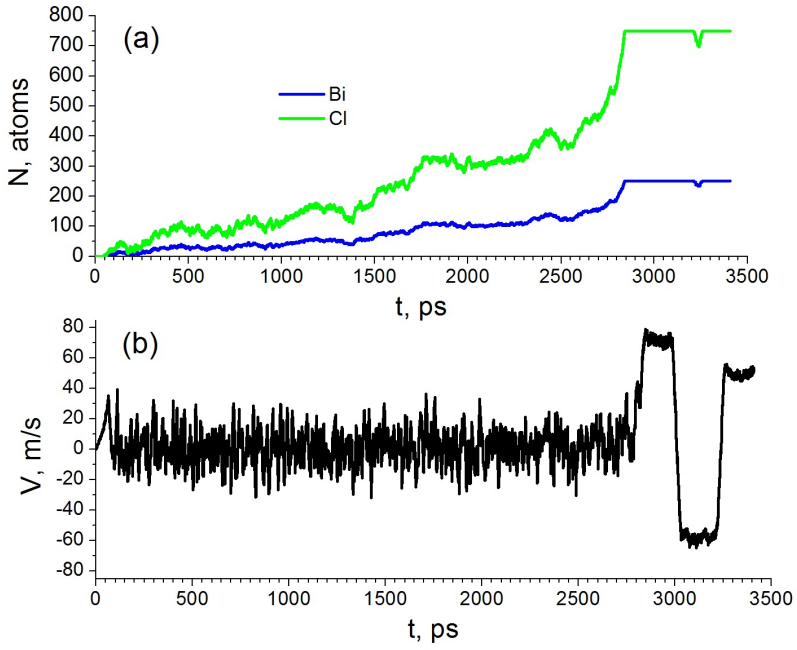

FIG. 7. Kinetics for imbibition of the $(BiCl_3)_{250}$ drop into a (20,20)@(25,25) DWCNT at $T = 623$ K: the number of atoms N penetrated into the cavity (a) and the velocity of the drop barycenter V (b) as functions of time t

Obviously, the long time required for penetration of a $BiCl_3$ drop into the narrow cavity of a DWCNT can be explained by a reorganization of internal structure of the melt. The comparison of the $g_{ij}(r)$ profiles for the melt within a nanotube and for the melt as free drop does not establish their essential difference. The structure of molten $BiCl_3$ preserves an amorphous character and is not affected by the nanotube wall. However, the mapping of angle-resolved radial distribution function unveils that, a Bi network within such $BiCl_3$ becomes more disorganized: a correlation between the Bi pairs disappears at distances more, than 7 Å, and is suppressed essentially at distance of 5 Å (Fig. 8a). Therefore, the structural reorganization of the melt is manifested through the progressive destruction of its chain-like Bi network during imbibition. Indeed, the size of a coiled or branched chain within the melt confined in a nanotube cavity is limited in one dimension by the inner diameter of the nanotube. The one-dimensional character of a nanotube imposes constraint on conformational variety for the labile chain-like structures of the melt, restricting their conformations allowed for imbibition to the mostly one-dimensional ones. Together with the destruction of chain-like Bi network in the drop outside of nanotube some time is required for the alignment of new chain-like Bi network in the drop inside the nanotube.

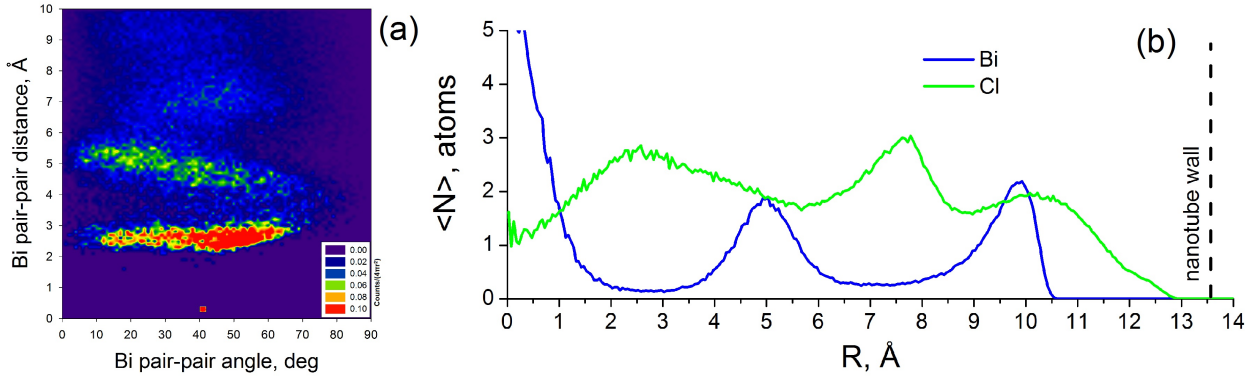

FIG. 8. Structural properties of the drop $(BiCl_3)_{250}$ embedded fully in the cavity of a (20,20)@(25,25) DWCNT after MD simulation at $T = 623$ K: (a) angle-resolved radial distribution function of the nearest-neighbor Bi–Bi pairs within the drop; (b) distribution of atoms along the radial direction of nanotube (R – the distance from the tube axis)

A view on the cross-section of final structure of the fully injected $BiCl_3$ melt along the DWCNT axis uncovers also a shell-like statistical distribution of the Bi and Cl atoms along radial direction (Fig. 8b). A clear alternation of the shells can be seen. At least in our model case, the core of the melt would mostly consist of Bi atoms, while the external part of the melt would consist of Cl atoms. A similar shell-like particles' distribution within a nanotube is typical also for other liquids assembled of either ions or non-polar molecules [31, 32, 34].

4. Summary

In summary, a facile capillary filling technique was tested for the fabrication of hybrid nanostructures $BiCl_3$@MWCNT – multi-walled carbon nanotubes filled with $BiCl_3$. Notwithstanding a relatively high surface tension of molten $BiCl_3$, the filling proceeds successfully at an elevated temperature of 350°C (∼115°C above the melting point of $BiCl_3$) and irrespective of the diameter distribution of MWCNTs. The encapsulated phase possesses a rod- or a tube-like morphology and is constituted by the pure and stoichiometric phase of orthorhombic $BiCl_3$.

The mechanism of imbibition of $BiCl_3$ by MWCNTs is considered at atomistic level and nanosecond time scale by means of molecular dynamics simulations, employing a force-field especially evaluated and approved for molten $BiCl_3$. The internal chain-like organization of molten $BiCl_3$ is recognized at an intermediate range order due to the correlation in dynamics of Bi–Bi pairs bridged via Cl atoms. In this sense, the $BiCl_3$ melt behaves very similar to an ionic melt with polyvalent cations, despite its molecular-like constitution. Such organization of molten $BiCl_3$ explains possibly its high surface tension as well the violation of the Lucas–Washburn rule for capillary filling into such narrow diameter capillaries like MWCNT. The imbibition of a $BiCl_3$ drop with the diameter larger, than the diameter of MWCNT host, requires a long induction period until diameters' equalization. Thereafter, the imbibition accelerates exponentially, finalizing in a frictionless cruise of the melt along the nanotubular channel and far away the entrance point.

The success of our study points to the opportunity of scalable production of $BiCl_3$@MWCNT hybrids as functional components of some eco-friendly catalysts for organic synthesis and as materials for nanodispersed radioprotective shielding.

Acknowledgement

E. A. A. and F. L. D. acknowledge the financial support by the N2020: Nanotechnology Based Functional Solutions (NORTE-01-0145-FEDER-000019), supported by Norte Portugal Regional Operational Program (NORTE2020), under the PORTUGAL 2020 Partnership Agreement, through the European Regional Development Fund (ERDF). A. E. recognizes the support from the Ural Branch of Russian Academy of Sciences via the multi-purpose program 18-10-3-32.

References

[1] Pederson M.R., Broughton J.Q. Nanocapillarity in Fullerene Tubules. *Physical Review Letters*, 1992, **69**, P. 2689–2692.
[2] Ajayan P.M., Iijima S. Capillarity-induced filling of carbon nanotubes. *Nature*, 1993, **361**, P. 333–334.
[3] Sloan J., Luzzi D.E., Kirkland A.I., Hutchison J.L., Green M.L. Imaging and Characterization of Molecules and One-Dimensional Crystals Formed within Carbon Nanotubes. *MRS Bulletin*, 2004, **29**, P. 265–271.
[4] Eliseev A.A., Kharlamova M.V., Chernysheva M.V., Lukashin A.V., Tretyakov Yu.D., Kumskov A.S., Kiselev N.A. Preparation and properties of single-walled nanotubes filled with inorganic compounds. *Russian Chemical Reviews*, 2009, **78**, P. 833–854.
[5] Gautam U.K., Costa P.M.F.J., Bando Y., Fang X., Li L., Imura M., Golberg D. Recent developments in inorganically filled carbon nanotubes: successes and challenges. *Sci. Technol. Adv. Mater.*, 2010, **11**, P. 054501.
[6] Hong S.Y., Kreizman R., Rosentsveig R., Zak A., Sloan J., Enyashin A.N., Seifert G., Green M.L.H., Tenne R. One- and Two-Dimensional Inorganic Crystals inside Inorganic Nanotubes. *European Journal of Inorganic Chemistry*, 2010, P. 4233–4243.
[7] Cabana L., Ballesteros B., Batista E., Magen C., Arenal R., Oro-Sole J., Rurali R., Tobias G. Synthesis of PbI_2 Single-Layered Inorganic Nanotubes Encapsulated Within Carbon Nanotubes. *Advanced Materials*, 2014, **26**, P. 2016–2021.
[8] Sandoval S., Pach E., Ballesteros B., Tobias G. Encapsulation of two-dimensional materials inside carbon nanotubes: Towards an enhanced synthesis of single-layered metal halides. *Carbon*, 2017, **123**, P. 129–134.
[9] Fidiani E., Costa P.M.F.J., Wolter A.U.B., Maier D., Buechner B., Hampel S. Magnetically Active and Coated Gadolinium-Filled Carbon Nanotubes. *The Journal of Physical Chemistry C*, 2013, **117**, P. 16725–16733.
[10] Anumol E.A., Enyashin A.N., Deepak F.L. Single Walled BiI_3 Nanotubes Encapsulated within Carbon Nanotubes. *Scientific Reports*, 2018, **8**, P. 10133.
[11] Sloan J., Kirkland A.I., Hutchison J.L., Green M.L.H. Integral atomic layer architectures of 1D crystals inserted into single walled carbon nanotubes. *Chemical Communications*, 2002, P. 1319–1332.
[12] Friedrichs S., Falke U., Green M.L.H. Phase Separation of LaI_3 inside Single-Walled Carbon Nanotubes. *ChemPhysChem*, 2005, **6**, P. 300–305.
[13] Fedoseeva Y.V., Orekhov A.S., Chekhova G.N., Koroteev V.O., Kanygin M.A., Senkovskiy B.V., Chuvilin A., Pontiroli D., Ricco M., Bulusheva L.G., Okotrub A.V. Single-Walled Carbon Nanotube Reactor for Redox Transformation of Mercury Dichloride. *ACS Nano*, 2017, **11**, P. 8643–8649.
[14] Nie C., Galibert A.-M., Soula B., Datas L., Sloan J., Flahaut E., Monthiox M. The unexpected complexity of filling double-wall carbon nanotubes with nickel (and iodine) 1D nanocrystals. *IEEE Transactions on Nanotechnology*, 2017, **16**, P. 759–766.
[15] Batra N., Anumol E.A., Smajic J., Enyashin A.N., Deepak F.L., Costa P.M.F.J. Morphological Phase Diagram of a Metal Halide Encapsulated in Carbon Nanotubes. *The Journal of Physical Chemistry C*, 2018 (submitted).
[16] Hong S.Y., Tobias G., Al-Jamal K.T., Ballesteros B., Ali-Boucetta H., Lozano-Perez S., Nellist P.D., Sim R.B., Finucane C., Mather S.J., Green M.L.H., Kostarelos K., Davis B.G. Filled and glycosylated carbon nanotubes for *in vivo* radioemitter localization and imaging. *Nature Materials*, 2010, **9**, P. 485–490.
[17] Spinato C., de Garibay A.P.R., Kierkowicz M., Pach E., Martincic M., Klippstein R., Bourgognon M., Wang J.T.-W., Menard-Moyon C., Al-Jamal K.T., Ballesteros B., Tobias G., Bianco A. Design of antibody-functionalized carbon nanotubes filled with radioactivable metals towards a targeted anticancer therapy. *Nanoscale*, 2016, **8**, P. 12626–12638.
[18] Adya A.K., Takagi R., Gaune-Escard M. Unravelling the Internal Complexities of Molten Salts. *Zeitschrift für Naturforshung A*, 1998, **53**, P. 1037–1048.
[19] Ravi K., Krishnakumar B., Swaminathan M. BiCl3-loaded montmorillonite K10: a new solid acid catalyst for solvent-free synthesis of bis(indolyl)methanes. *Research on Chemical Intermediates*, 2015, **41**, P. 5353–5364.
[20] Patil V.D., Sutar N.R., Patil K.P., Giddh P. $BiCl_3$ - an eco-friendly catalyst for an efficient synthesis of benzoxazoles at room temperature. *Chemistry of Heterocyclic Compounds*, 2015, **51**, P. 1019–1022.
[21] Diemer R., Dittes U., Nuber B., Seifried V., Opferkuch W., Keppler B.K. Synthesis, Characterization and Molecular Structures of some Bismuth(III) Complexes with Thiosemicarbazones and Dithiocarbazonic Acid Methylester Derivatives with Activity against Helicobacter Pylori. *Metal-Based Drugs*, 1995, **2**, P. 271–292.
[22] Marcus Y. *Ionic Liquid Properties: From Molten Salts to RTILs*. Springer International Publishing, 2016, 244 p. ISBN 978-3-319-30313-0
[23] Friedman R.M., Corbett J.D. On the Synthesis and Crystal Structure of Dodecabismuth Tetradecachloride, $Bi_{12}Cl_{14}$. *Inorganica Chimica Acta*, 1973, **7**, P. 525–527.
[24] Bartl H. Meßzeitersparnis durch Profilauswertung bei der Registrierung von Neutroneneinkristallreflexen. Die Kristallstruktur von Wismuttrichlorid, $BiCl_3$. *Fresenius' Zeitschrift für analytische Chemie*, 1982, **312**, P. 17–18.
[25] Rappé A.K., Casewit C.J., Colwell K., Goddard III W., Skiff W., UFF, a Full Periodic Table Force Field for Molecular Mechanics and Molecular Dynamics Simulations. *Journal of American Chemical Society*, 1992, **114**, P. 10024–10035.

[26] Imperatori P., Ferro D., Piacente V. Sublimation study of $BiCl_3$ and of $BiBr_3$. *The Journal of Chemical Thermodynamics*, 1982, **14**, P. 461–472.
[27] Clay A.T., Kuntz C.M., Johnson K.E., East A.L.L. The origin of the conductivity maximum in molten salts. I. Bismuth chloride. *Journal of Chemical Physics*, 2012, **136**, P. 124504.
[28] Humphrey W., Dalke A., Schulten K. VMD: Visual molecular dynamics. *Journal of Molecular Graphics*, 1996, **14**, P. 33–38.
[29] Töke O., Hargittai M. Molecular Structure of Bismuth Trichloride from Combined Electron Diffraction and Vibrational Spectroscopic Study. *Structural Chemistry*, 1995, **6**, P. 127–130.
[30] Denchik E., Nyburg S.C., Ozin G.A., Szymanski J.T. Raman Spectra of Gaseous, Liquid, and Solid Bismuth Trichloride: Resonance Fluorescence Spectra of gaseous BiCl and BiBr. *Journal of the Chemical Society A*, 1971, **0**, P. 3157–3159.
[31] Deepak F.L., Enyashin A.N. Capillary Imbibition of Gadolinium Halides into WS_2 Nanotubes: a Molecular Dynamics View. *Israel Journal of Chemistry*, 2017, **57**, P. 501–508.
[32] Enyashin A.N., Kreizman R., Seifert G. Capillary Imbibition of PbI_2 Melt by Inorganic and Carbon Nanotubes. *The Journal of Physical Chemistry C*, 2009, **113**, P. 13664–13669.
[33] Anumol E.A., Enyashin A.N., Batra N.M., Costa P.M.F.J., Deepak F.L. Structural and chemical analysis of gadolinium halides within WS_2 nanotubes. *Nanoscale*, 2016, **8**, P. 12170.
[34] Goldbart O., Cohen S.R., Kaplan-Ashiri I., Glazyrina P., Daniel Wagner H., Enyashin A., Tenne R. Diameter-dependent wetting of tungsten disulfide nanotubes. *Proceedings of the National Academy of Sciences*, 2016, **113**, P. 13624–13629.